Transverse turbulent bands in rough plane Couette flow

Takahiro Tsukahara, Takeru Tomioka, Takahiro Ishida, Yohann Duguet, Geert Brethouwer

Bulletin of the JSME Vol.13, No.3, 2018
Journal of Fluid Science and Technology

Transverse turbulent bands in rough plane Couette flow

Takahiro TSUKAHARA*, Takeru TOMIOKA*, Takahiro ISHIDA**, Yohann DUGUET*** and Geert BRETHOUWER****

* Department of Mechanical Engineering, Tokyo University of Science
2641 Yamazaki, Noda-shi, Chiba 278-8510, Japan
E-mail: tsuka@rs.tus.ac.jp
** Aeronautical Technology Directorate, Japan Aerospace Exploration Agency (JAXA)
6-13-11 Osawa, Mitaka, Tokyo 181-0015, Japan
*** LIMSI-CNRS, Campus Universitaire d'Orsay
Université Paris-Saclay, F-91405 Orsay, France
**** Linné Flow Centre, KTH Mechanics
SE-10044 Stockholm, Sweden

Received: 2 April 2018; Revised: 20 July 2018; Accepted: 27 August 2018

Abstract

In most subcritical planar shear flows, the transitional regime features oblique large-scale laminar-turbulent patterns. So far, such laminar-turbulent patterns have only been investigated in flows over perfectly smooth walls and little attention has been devoted to cases with rough surfaces as found in most practical engineering, urban applications, and in nature. In this study, we investigate laminar-turbulent patterns in plane Couette flow with one rough wall by means of direct numerical simulation, as a function of the Reynolds number and of the roughness height. The roughness is modeled using a force term in the Navier–Stokes equations. The focus of this study is on a new regime featuring non-oblique turbulent bands transverse to the motion of the walls, and separated by arbitrary long laminar gaps. This regime is found when the wall is sufficiently rough. This transverse turbulent band occurs at Reynolds numbers just below the onset of self-sustained turbulence found in the smooth wall case. The localized turbulence patches have a streamwise extent as large as 50–180 gap widths, decreasing with decreasing Reynolds number. The turbulent fraction as well as the band width show a linear relationship with the Reynolds number.

Keywords : DNS, Canopy flow, Intermittency, Laminar-turbulence coexistence, Plane Couette flow, Roughness, Subcritical transition, Turbulent stripe, Wall-bounded turbulence

1. Introduction

Most wall-bounded shear flows become turbulent following a subcritical transition scenario. A striking consequence of the competition between laminar and turbulent dynamics is the possibility of spatial coexistence of laminar flow and sustained turbulent patches at the lowest Reynolds numbers, see the comprehensive review by Manneville (2016). Investigation of such coexistence regimes becomes demanding in terms of statistics near the lowest limit in terms of the Reynolds number, where the turbulent fraction becomes small and the flow field exhibits strong intermittency in both space and time (Shi et al., 2013; Lemoult et al., 2016; Sano & Tamai, 2016; Chantry et al., 2017; Mukund & Hof 2018). In plane Couette flow, the transitional regime occurs for $1300 \leq \mathrm{Re_w} \leq 1600$, where $\mathrm{Re_w} = U_w d/\nu$ is based on the relative wall velocity U_w, the channel gap d, and the kinematic viscosity ν. It features oblique large-scale laminar-turbulent stripe patterns that proliferate in the homogenous directions (Prigent et al., 2002; Barkley & Tuckerman, 2005; Tsukahara et al, 2009; Duguet et al., 2010; Tuckerman & Barkley, 2011). Each turbulent band has well-defined width and angle with respect to the mean flow direction. The wavelength of the patterns and the oblique angle of the bands vary gently with the Reynolds number. Similar stripe patterns can occur in higher Reynolds number flows, in the presence of either stable stratification or Coriolis forces. Even in such cases, the turbulent bands are oblique and have an angle comparable to those in the neutrally-stratified flow (Tsukahara et al., 2010; Tsukahara, 2011; Brethouwer et al., 2012). Despite recent progress

Paper No.18-00159
[DOI: 10.1299/jfst.2018jfst0019]

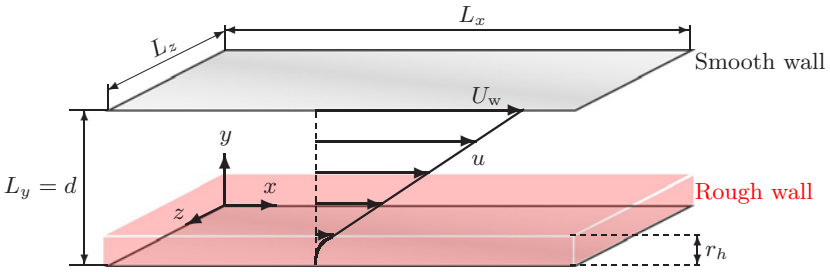

Fig. 1 Configuration of plane Couette flow with a rough fixed bottom wall.

in elucidating the mechanisms for the observed obliqueness (Duguet & Schlatter, 2013), several points still remain to be better understood and quantified like the physical reasons for the laminar-turbulent coexistence, its self-organization, and its dynamics.

Most experimental studies of wall-bounded shear flows were performed with carefully designed smooth walls, while numerical studies of the laminar-turbulent pattern have exclusively focused on perfectly smooth walls. However, practical/natural solid surfaces in engineering applications feature wall roughness. A crucial issue here is the robustness of the laminar-turbulent patterning in the presence of wall roughness. This task involves a clear cartography of the regime of laminar-turbulent patterns in a parameter space including the parametrization of the roughness elements.

Ishida et al. (2017) studied numerically the transitional regime of plane Couette flow with rough walls by adding a body force mimicking the roughness effect. The competition between the induced body force and shear-induced instabilities led to a variety of transition sequences and structures. The main parameters that were varied in their simulation were the roughness height and the Reynolds number. They determined the flow states in the parameter space spanned by these two parameters using the numerical observations. An interesting prospect arising from the work of Ishida et al. (2017) is that the localized turbulence can form a non-oblique pattern when one wall is sufficiently rough. Such a plane Couette flow is asymmetric since one wall is rough and the other smooth. They actually reported a transverse turbulent band (TTB, hereafter) that was perpendicular to the motion of the walls in the range $\mathrm{Re_w} = 900$–1000, instead of the oblique turbulent band (OTB) expected for the subcritical transition scenarios between smooth walls.

In this study, by means of direct numerical simulation (DNS) of plane Couette flow with one strongly rough wall, the size of the TTB and its dependence on the Reynolds number are investigated. In addition, we refine the parameter space for the formation of the TTB. Smooth plane Couette flow is a convenient prototype for the study of subcritical transition, since its base flow has a simple analytical expression that is linearly stable for all values of the Reynolds number. We employ a periodic numerical domain large enough to accommodate at least one wavelength of a laminar-turbulent pattern in the transitional range. The choice of rough Couette flow is motivated by the following reasons : the smooth wall case is well documented in the literature with respect to pattern formation, and this configuration is realistic as attested by several experimental studies (Prigent et al., 2002; Tsukahara et al., 2010; Couliou & Monchaux, 2017). The roughness effect on other shear flows with laminar-turbulent intermittency deserves separate studies. In the present investigation, the roughness is distributed along one wall only and is modelled numerically using a parametric model suggested recently in the context of higher-*Re* shear flows (Busse & Sandham, 2012).

2. Flow case and numerical procedure

We consider fully-developed plane Couette flow (pCf), i.e., the flow sheared between two parallel infinite plates moving with respective velocities 0 and U_w in the x direction. The two walls are separated by a gap d in the y direction normal to the walls. A rough surface is assumed only on the static bottom wall at $y = 0$, while the moving wall at $y = d$ is considered perfectly flat. Figure 1 schematically illustrates the flow configuration, the spanwise direction being denoted as z. The computational domain has size $L_x \times L_y \times L_z$, and periodic boundary conditions are applied in both x and z directions.

The flow, i.e., the velocity field $[u, v, w](x, y, z, t)$ and the pressure $p(x, y, z, t)$, are governed by the incompressible Navier–Stokes equations with no-slip boundary conditions at the walls, but for the rough case the governing equations are modified by the addition of a volumetric drag force term. The roughness effect is incorporated in our own DNS code without any change in the boundary conditions and the Cartesian grid system. The modified Navier–Stokes equation (with

[DOI: 10.1299/jfst.2018jfst0019]

Table 1 Main parameters and numerical conditions.

			Reference domain ($L_y = d$)		Long domain ($L_y = d$)				
$\mathrm{Re_w}$	h/d	$\alpha_i d$	$L_x \times L_z$	$N_x \times N_y \times N_z$	$L_x \times L_z$	$N_x \times N_y \times N_z$	Δx^+, Δz^+	$\Delta y^+_{\max}$	$\Delta y^+_{\min}$
800–1000	0.2	1.0	$136d \times 68d$	$1024 \times 96 \times 512$	$544d \times 34d$	$4096 \times 96 \times 256$	2.35–3.19	0.43–0.58	0.018–0.024

time t and the density ρ) reads

$$\frac{\partial u_i}{\partial t} + u\frac{\partial u_i}{\partial x} + v\frac{\partial u_i}{\partial y} + w\frac{\partial u_i}{\partial z} = -\frac{1}{\rho}\frac{\partial p}{\partial x_i} + \nu\left(\frac{\partial^2 u_i}{\partial x^2} + \frac{\partial^2 u_i}{\partial y^2} + \frac{\partial^2 u_i}{\partial z^2}\right) - \alpha_i F_i(y)|u_i|u_i. \tag{1}$$

The last term on the right-hand side represents the additional drag force induced by all roughness elements together. It is exactly the body force used by Busse & Sandham (2012) to model the effect of roughness. Note that the summation convention with respect to $(\cdot)_i$ does not apply for this term in Eq. (1), in which α_i is the roughness factor and F_i the roughness shape function according to the terminology of Busse & Sandham (2012). That force on a unit volume alone also reads

$$\begin{cases} -\rho\left(\alpha_x u|u|, \alpha_y v|v|, \alpha_z w|w|\right) & \text{if} \quad y \le r_h = 2h, \\ (0,0,0) & \text{if} \quad y > r_h = 2h. \end{cases} \tag{2}$$

This term is quadratic with respect to the velocity field, inducing a dominant form drag expected at high Reynolds numbers to scale with the dynamic pressure. Drag terms of a comparable form $-|\mathbf{u}|u_i$ were used in several numerical studies of atmospheric boundary layer flows over plant canopies (Su et al., 1998; Finnigan, et al., 2009). In our study, we chose the expression $-|u_i|u_i$ suggested by Busse & Sandham (2012). Such a form ensures that this term always plays a damping role against the flow motions near the rough surface. The roughness factor α accounts for the spatial density (with a unit of m^{-1}) of unspecified roughness elements, therefore the model should be considered as a statistical one. We chose $\alpha_x = \alpha_y = \alpha_z = 1$ (corresponding to a mildly dense array of roughness elements) and we confirmed that the present results are qualitatively insensitive to variations in α. The shape function F_i models the wall-normal distribution of the roughness elements. Based on the original study by Busse & Sandham (2012), we employ a simple box profile:

$$F_i(y) = \begin{cases} 1 & \text{if} \quad y \le r_h = 2h \\ 0 & \text{if} \quad y > r_h = 2h \end{cases} \tag{3}$$

with r_h the height of the roughness sublayer above which the drag term vanishes, see Fig. 1. In the following, as in previous studies, we use a mean height h to describe the roughness height. As for the profile given by Eq. (3), $h = r_h/2$. Another Gaussian profile for F_i was also tested in Ishida et al. (2017). No significant qualitative difference in phenomenological results was found using the two different profiles for $F_i(y)$.

The governing equations include the equation of continuity

$$\frac{\partial u_j}{\partial x_j} = 0, \tag{4}$$

are coupled by the fractional step method, and discretized using finite differences, namely a fourth-order central scheme in the x and z directions and a second-order scheme in the y direction with a non-uniform grid. Time advancement was carried out using the second-order Adams–Bashforth method, whereas the second-order Crank–Nicolson method was used for the viscous term in y. The pressure Poisson equation is solved in Fourier space using fast Fourier transforms in x and z, and a tridiagonal solver was employed in y. The DNS code was adapted and validated in earlier studies of fully turbulent and transitional pCf with smooth walls (Tsukahara et al., 2006, 2009).

The parametric study was conducted in a range of $\mathrm{Re_w}$=750–1200 and h=0.075–0.25d, aiming at a comprehensive picture of the complex variations in flow state and structure in rough pCf. The domain $L_x \times L_y \times L_z$ was set to $136d \times d \times 68d$ using a grid with $N_x \times N_y \times N_z = 1024 \times 96 \times 512$ points. This size was selected after preliminary DNSs with different computational domains, as described in Section 3.2. The present basic domain is larger than that of Ishida et al. (2017) and sufficient to capture the OTB, whose structure displays long correlations in both x and z directions, of the order of $10d$–$100d$. The main purpose is a deeper investigation of the new regime characterized by the TTB identified in Ishida et al. (2017). In order to capture such a one-dimensional coherent structure, which may show long correlation in x but not in z, a long (in x) and narrow (in z) computational domain would be reasonable in the context of limited computational resources. A domain size of $544d \times d \times 34d$ was chosen for the additional numerical investigation of TTB in a more limited parameter range $(\mathrm{Re_w}, h/d) = (800\text{–}1000, 0.2)$, where the appearance of the TTB is expected.

[DOI: 10.1299/jfst.2018jfst0019]

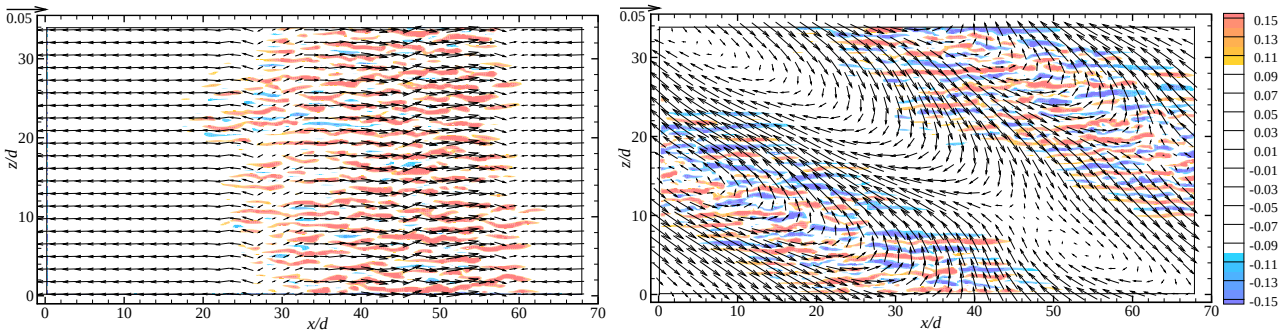

(a) TTB for $\mathrm{Re_w} = 1000$ and $h/d = 0.2$

(b) OTB for $\mathrm{Re_w} = 1100$ and $h/d = 0.1$

Fig. 2 Two-dimensional contours of instantaneous u'/U_w shown by colours and low-pass filtered large-scale flow (U, W) shown as vectors at $y/d = 0.5$. The contour levels are the same in the two figures, and the reference-vector length is shown in the top left corner of each panel.

Table 1 summarizes the numerical conditions especially for the main investigation of the TTB, including the grid resolution Δx_i^+ in wall units. The present resolutions are comparable to those used by Busse & Sandham (2012), and are fine enough to capture fine-scale near-wall eddies as well as the large-scale laminar-turbulent patterns. Note that the usual oblique patterns are numerically robust in this range of parameters, according to the extended resolution study by Manneville & Rolland (2011). The time increment Δt is small enough to satisfy the Courant-Friedrichs-Lewy criterion ($u_j \Delta t / \Delta x_j < 0.5$).

3. Results and discussion

3.1. Transverse turbulent band (TTB)

Figures 2(a) and 2(b) display in-plane visualizations of a TTB and an OTB (oblique turbulent band) found at $(\mathrm{Re_w}, h/d) = (1000, 0.2)$ and $(\mathrm{Re_w}, h/d) = (1100, 0.1)$, respectively. Here, the domain size of $L_x \times L_y \times L_z = 68d \times d \times 34d$ is the same as in Ishida et al. (2017). Both figures reveal a single band of localized turbulence with a streamwise width of about $30d$. Inside the turbulent band, we can see many quasi-streamwise streaks of length less than $20d$ and spanwise spacing of $\mathrm{O}(d)$. This streak cluster allows us to recognize the macroscopic laminar-turbulent interfaces. The laminar-to-turbulent (L→T with respect to x) and turbulent-to-laminar (T→L) interfaces in Fig. 2(a) are along the z-axis, while they are parallel to the domain diagonal in Fig. 2(b). The OTB has an oblique angle of 27° (= $\tan^{-1} 0.5$) with the x axis, which is a typical order of magnitude reported by several teams (see Tuckerman & Barkley, 2011 and references therein).

Besides the angle of the laminar-turbulent interface, there are other strong differences between TTB and OTB. As can be seen in Fig. 2, the intensity of the streaks differ between the two cases. For the isovalues displayed at $y/d = 0.5$, whereas in Fig. 2(b) both low- and high-speed streaks can be seen along both laminar-turbulent interfaces for the OTB, in Fig. 2(a) only the most intense streaks can be seen at the interfaces of the TTB. Note here that, by convention, the impermeable wall is located at $y = 0$ (no virtual origin), while the smooth wall is at $y/d = 1$. The current asymmetry with respect to y does not allow to make meaningful comparisons at the exact mid-gap value of $y/d = 0.5$. Instead, the velocity contours might be plotted at the apparent mid-gap value defined by the minimum of $\partial u_x(y)/\partial y$ for $y \geq r_h$ (above the rough region), but such a procedure would make the comparison of the cases with different roughness heights more complex.

In addition to the above-mentioned difference in the streaks observed inside the turbulent regions, the accompanying large-scale flow (LSF) is qualitatively different between the two cases. Figure 2 shows velocity vectors of a low-pass filtered instantaneous field for each case. The LSF is obtained by the application of a low-pass filter that selects only the lowest-order modes in the x and z directions. The spectral cutoff criterion was chosen to extract the modes $(m_x, m_z) = (0, \pm 1), (\pm 1, 0), (\pm 1, \pm 1)$, and $(\pm 2, 0)$ in this post processing. The exact choice of the filter kernel matters little as long as the scale separation between the fine-scale structures such as streaks and the LSF is sufficiently large. As clearly seen in Fig. 2, the LSF in the case of the OTB has a significant spanwise component, which is absent in the case with the TTB. More specifically, Fig. 2(b) demonstrates that a spanwise LSF component exists, directed towards negative z around the L→T interface of the OTB and in the opposite direction near the T→L interface. This large-scale spanwise flow along the band is a key feature of the OTB (Duguet & Schlatter, 2013). The case with the TTB, presented in Fig. 2(a), does not feature a LSF in the spanwise direction (or along the band). This deviation of the LSF at the interfaces may be explained by the presence of the roughness region, as proposed in the previous paper (Ishida et al., 2017). On the other hand, the streamwise component of the LSF for both the TTB and OTB has a similar magnitude and pattern. Further investigations

[DOI: 10.1299/jfst.2018jfst0019]

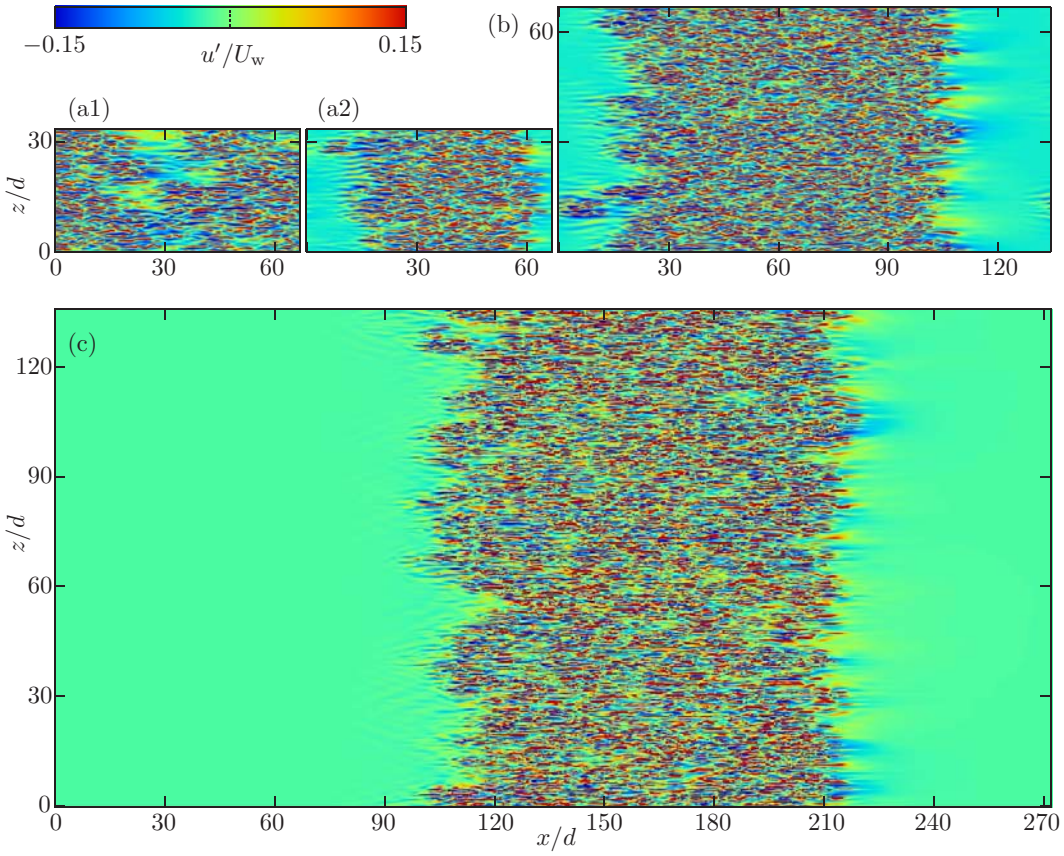

Fig. 3 Visualizations of the instantaneous streamwise velocity in the x-z plane at $y/d = 0.5$ for $\mathrm{Re_w} = 1000$ and $h/d = 0.2$ in DNS with different domain sizes. Contours are normalized by the wall speed U_w. In the subfigures (a1) and (a2) the domain size is $L_x \times L_z = 68d \times 34d$, in (b) $136d \times 68d$, and in (c) $272d \times 136d$.

of the LSF and its relevance to the mechanisms of TTB and OTB will be presented in future works.

We may notice that the turbulent band is wider for the TTB than for the OTB, see Fig. 2, although the Reynolds number is lower in the former case. Wider turbulent bands correspond to a larger turbulent fraction, which suggests that a decreasing Reynolds number delays the decaying process. The increased turbulent fraction, seen in the TTB case for $h/d = 0.2$, compared to the case with the OTB and $h/d = 0.1$, implies an enhancement of the velocity fluctuations (i.e. the streaks) by the wall roughness. The Reynolds number dependence of the band width and the turbulent fraction for fixed $h/d = 0.2$ will be discussed in Sections 3.3 and 3.4.

3.2. Domain size versus band width

As described in Section 3.1, an OTB evolves into a TTB by slightly changing the parameters. In order to verify that the regime of TTB is *not* an artefact of the spatial periodicity assumption, larger additional DNSs have been performed for $(\mathrm{Re_w}, h/d) = (1000, 0.2)$, for which Ishida et al. (2017) reported a flow state with one or several laminar spots evolving in a turbulent environment, rather than a well-organized turbulent band. However, the present DNS reveals a TTB as the final flow state at equilibrium for the same parameter set, as reported in this section. This finding motivated us to carry out the following longer simulations inside larger computational domains.

All results shown in Fig. 3 are for the same values of $\mathrm{Re_w}$ and h, only the computational domain size is varied. The Reynolds number was initially $\mathrm{Re_w} \geq 1100$ in all DNS in order to provide a fully-turbulent initial flow field (without any macroscopic intermittency), then instantaneously decreased and kept at 1000. We confirm that the decaying turbulent flow actually reveals 'laminar spots' at an early stage shown in Fig. 3(a1), as observed by Ishida et al. (2017); however a TTB appears eventually, as shown in Fig. 3(a2) after a time of $2500d/U_w$. The laminar spots have thus finite lifetimes and recurrently regenerate from the fluctuating turbulent environment. After a long transient phase, the flow reaches an organized laminar-turbulent pattern with a TTB. The streamwise width of the TTB given in (a2) is almost comparable with the domain size. We decided to perform a DNS with a quadrupled domain size (lengths both in x and z were doubled) : a single TTB was again observed, as shown in Fig. 3(b). One might expect two bands to appear in the domain twice as

[DOI: 10.1299/jfst.2018jfst0019]

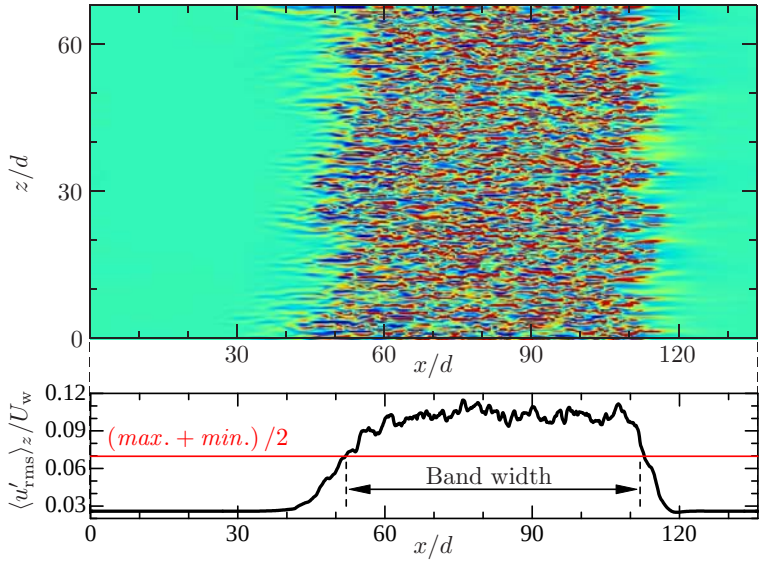

Fig. 4 (top) Visualizations of the instantaneous streamwise velocity in the x-z plane at $y/d = 0.5$ for $\mathrm{Re_w} = 900$, $h/d = 0.2$, and the reference domain. The contour range is the same as in Fig. 3. (bottom) Corresponding profile of $\langle u'_{\mathrm{rms}} \rangle_z$ as a function of x.

long as the smaller one shown in (a2), but interestingly the band width itself doubled in the large domain in (b). Indeed, the obtained turbulent fractions, $F_t \approx 0.6$, for both (a2) and (b) are comparable to each other. Here, the turbulent fraction F_t, which measures the amount of turbulence in the flow field, is time-averaged from x-z plane data at mid-gap. The criterion for distinguishing laminar regions from turbulence is the wall-normal velocity and its threshold value is defined by $|v| < 0.003U_w$ (laminar) vs. $|v| > 0.003U_w$ (turbulent). The fully turbulent state corresponds to $F_t \approx 1$, while $F_t = 0$ corresponds to the globally laminar state. When the domain was further extended to $L_x \times L_z = 272d \times 136d$, we found a wider laminar region and almost constant band width, as shown in Fig. 3(c). Such a relatively large laminar flow region results in a decreased F_t, which actually drops to half of that in (b). It must be noted that the same number of grid points was used in the cases shown in (b) and (c), but the grid resolution for the largest domain in (c) were still good: Δx^+ and $\Delta z^+ \approx 6$. The smaller TTB observed in (a2) must be due the limitations in L_x. From this domain-dependency study, we conclude that, although both the band width and the size of the laminar region may depend on the domain size, the TTB is an intrinsic state, and that the exact band width can be estimated if the domain is long enough. In the following study, $L_x \times L_z = 136d \times 68d$ was chosen as our reference domain, which appears sufficient to capture the TTB.

Figure 4 shows a flow field accompanied by a slightly narrower band compared to that in Fig. 3(b), with the same roughness height but lower $\mathrm{Re_w}$, as another example of a flow with a TTB. We now introduce a way of determining the band width quantitatively. We use a value of $\langle u'_{\mathrm{rms}} \rangle_z$, which is computed as

$$\langle u \rangle_{xz}(y,t) = \frac{1}{L_x L_z} \int_0^{L_x} \int_0^{L_z} u(x,y,z,t) \mathrm{d}x\mathrm{d}z, \tag{5}$$

$$u'(x,y,z,t) = u(x,y,z,t) - \langle u \rangle_{xz}(y,t), \tag{6}$$

$$\langle u'_{\mathrm{rms}} \rangle_z(x,y,t) = \left\{ \frac{1}{L_z} \int_0^{L_z} [u'(x,y,z,t)]^2 \, \mathrm{d}z \right\}^{\frac{1}{2}}. \tag{7}$$

Its streamwise variation for the snapshot shown in Fig. 4 is displayed at the bottom of the figure. Based on this, one may easily distinguish turbulent from laminar regions. Note that $\langle u'_{\mathrm{rms}} \rangle_z$ is not zero in the laminar region because of the LSF. In the turbulent region, $\langle u'_{\mathrm{rms}} \rangle_z$ levels off at about $0.1U_w$ with small variations. Between turbulent and laminar regions, $\langle u'_{\mathrm{rms}} \rangle_z$ grows or decays over streamwise distances of $10d$–$20d$. We suggest a threshold equivalent to the median value between maximum and minimum of $\langle u'_{\mathrm{rms}} \rangle_z$. We define the points where $\langle u'_{\mathrm{rms}} \rangle_z$ crosses this threshold line as the begin and end points of the TTB. From this the width of TTB is determined. The obtained values and their dependences on the Reynolds number and domain size will be discussed in Section 3.4.

3.3. Flow map: TTB regime

A parametric DNS study of pCf with one rough wall, as illustrated in Fig. 1, was conducted with two control parameters $\mathrm{Re_w}$ and h, following an adiabatic decrease procedure in $\mathrm{Re_w}$. This computational strategy of 'adiabatic decrease'

[DOI: 10.1299/jfst.2018jfst0019]

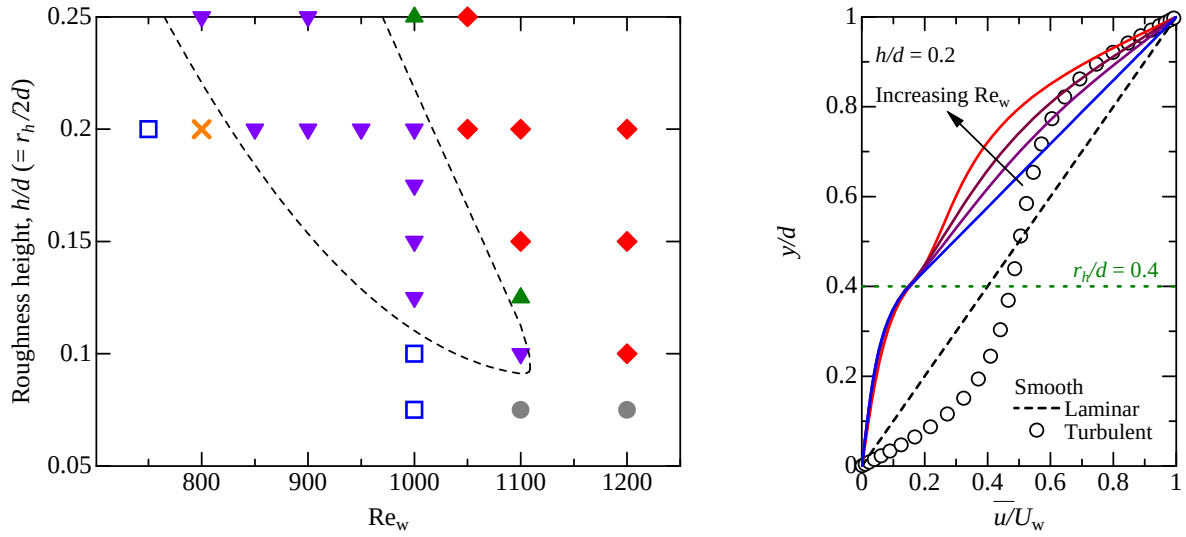

(a) Flow map (b) Mean velocity

Fig. 5 General flow properties of one rough-wall plane Couette flow in DNS with a domain size of $L_x \times L_z = 136d \times 68d$. (a) State transition diagram in terms of the Reynolds number and the roughness height; ♦ featureless turbulence, □ laminar, ● OTB (oblique turbulent band), ▼ TTB (transverse turbulent band), ▲ laminar spot in turbulent environment, × staggered vortex pattern. (b) Mean streamwise velocity profiles for $h/d = 0.2$. - - - smooth plane Couette flows at $\mathrm{Re_w} = 1200$ (laminar state), ○ at $\mathrm{Re_w} = 2000$ (turbulent state). Solid lines represent rough-wall cases at $\mathrm{Re_w} = 1100$ (red), 1000, 900, and 800 (blue).

is such that we first prepare a turbulent flow at sufficiently high $\mathrm{Re_w}$, then decrease $\mathrm{Re_w}$ stepwise down to the desired value, and after each step continue the simulation until statistical equilibrium is reached. This adiabatic procedure, which allows to estimate the critical point in $\mathrm{Re_w}$ for the sustenance of turbulence in a given finite-size system, is carried on until full laminarization occurs. The map of flow regimes is shown in Fig. 5(a). Using the expanded domain, we have revised the previous map by Ishida et al. (2017) by adding a few points near $(\mathrm{Re_w}, h/d) = (1000, 0.2)$. For such parameters we confirm the formation of a TTB after a transient phase consisting of laminar spots, as reported in Section 3.2.

For $h/d \leq 0.05$, the situation is unchanged compared to the smooth wall case (figure not shown here). For $h/d > 0.05$, the apparent value of the lower critical Reynolds number decreases monotonically with increasing h. The OTB regime (represented by gray bullets in Fig. 5(a)) is found to be robust for, at least, $h/d \leq 0.075$ in the range of $\mathrm{Re_w} = 1100$–1200, but they are no longer encountered at $\mathrm{Re_w} < 1100$ for $h > 0.1$. At $(\mathrm{Re_w}, h/d) = (1100, 0.1)$ we detected a zigzagging TTB, i.e., an intermediate shape between TTB and OTB, while a small domain captured a proper OTB (see Fig. 2(b)). In the regime of featureless turbulence at higher $\mathrm{Re_w}$, the flow field is dominated by coherent streamwise streaks in the whole domain. Flow visualizations of such states can be seen in Ishida et al. (2017). The zone delimited by a dashed line marks the TTB regime. This regime appears a precursor to full-fledged turbulence at high Reynolds numbers, at least for the current value of α. In the following, flow fields at a fixed $h/d = 0.2$ but varying $\mathrm{Re_w}$ are visualized and discussed with an emphasis on the laminar-turbulent pattern.

Figure 5(b) shows the mean velocity profiles averaged in x, z, and t. Only the cases at $(\mathrm{Re_w}, h/d) = (800$–$1000, 0.2)$ are plotted, but the profiles for the laminar and fully turbulent smooth wall cases are also included for reference. The wall-normal position of the equivalent roughness crest is at $0.4d$, below which the profiles are found to be independent of the Reynolds number. As the Reynolds number increases, the roughness-free region exhibits a tendency toward more turbulent-like profile with a higher shear rate at the top wall. Figure 6 shows that for $h/d = 0.2$ the TTB is not only found at $\mathrm{Re_w} = 1000$ but also at $\mathrm{Re_w}$ down to 850, whereas at $\mathrm{Re_w} = 1100$ the flow is fully turbulent. The streamwise extent of the TTB at equilibrium is found to monotonically decrease as $\mathrm{Re_w}$ decreases from 1000 to 850. The structure of the laminar-turbulent interfaces as well as the local turbulent intensity inside the TTB do not change as the TTB becomes smaller. The shrinking of the TTB means that the mean turbulent fraction at equilibrium declines with $\mathrm{Re_w}$. These variations of the turbulent fraction with $\mathrm{Re_w}$ will be further examined in Section 3.4. At $(\mathrm{Re_w}, h/d) = (800, 0.2)$, turbulence is absent and we instead observe a regular pattern of very weak disturbances, much weaker than the typical turbulent fluctuations. The mean streamwise velocity profile almost linear throughout the roughness-free region, as shown in Fig. 5(b). The cause of this regular pattern is yet unknown, but we may speculate that it is related to a weakly saturated linear instability.

[DOI: 10.1299/jfst.2018jfst0019]

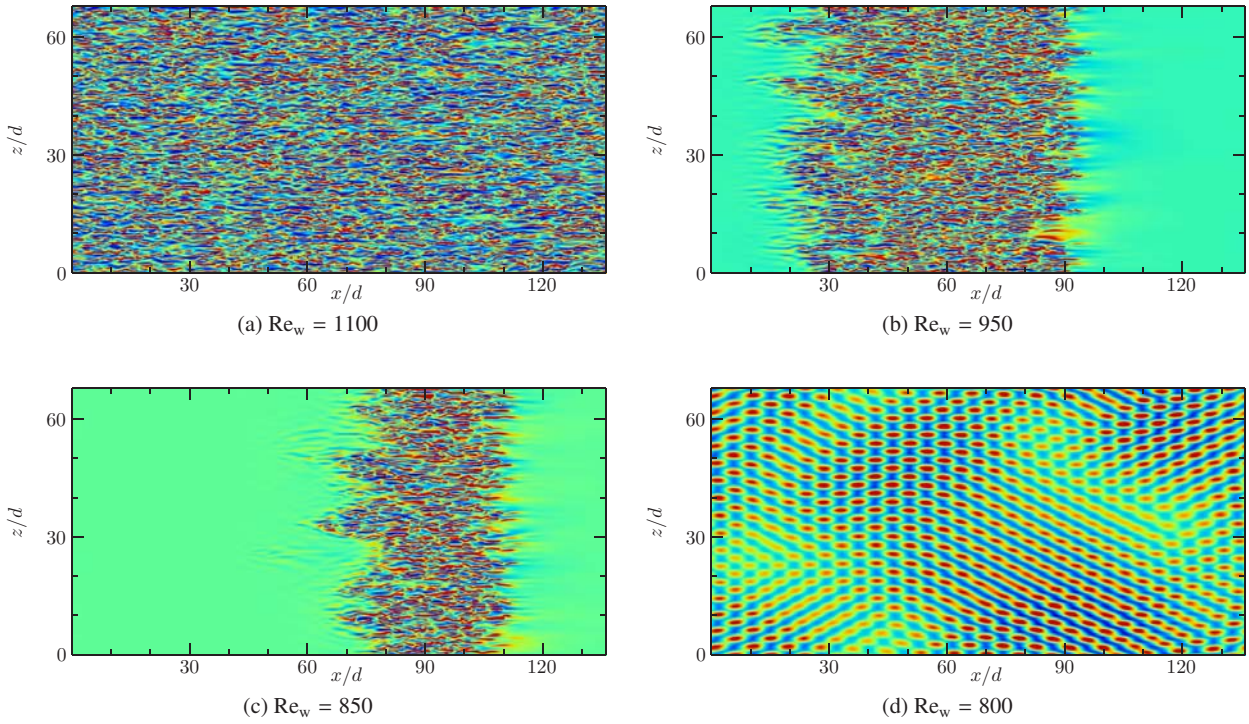

(a) $\mathrm{Re_w} = 1100$ (b) $\mathrm{Re_w} = 950$

(c) $\mathrm{Re_w} = 850$ (d) $\mathrm{Re_w} = 800$

Fig. 6 Two-dimensional contours of typical instantaneous u' distributions in the x-z plane at $y/d = 0.5$ for $h/d = 0.2$. Contours range from $-0.15U_\mathrm{w}$ (blue) to $0.15U_\mathrm{w}$ (red) for (a)–(c), as in Fig. 3; but from $-0.015U_\mathrm{w}$ to $0.015U_\mathrm{w}$ for (d).

3.4. Reynolds number dependence of the turbulent fraction

As demonstrated previously, the spanwise extent of the computational domain does not appear to have a critical influence on the appearance of TTBs whereas the streamwise extent does. This motivated us to carry out additional DNSs with a narrower but significantly longer computational domain where h was kept the same as in the DNS visualized in Fig. 6, i.e., $h/d = 0.2$. We refer to Table 1 for the numerical parameters of the long domain simulations. Each flow state was again achieved via an adiabatic decrease. Visualizations of the flow field for DNSs in the long domain are shown in Fig. 7. As before, the flow is fully turbulent at $\mathrm{Re_w} = 1100$. However, at $\mathrm{Re_w} = 900$ and 1000 we observe two TTBs instead of one as in the DNS with a shorter domain. These TTBs travel downstream at a constant speed, and because all fronts move with the same velocity concurrent TTBs do not collide or merge. Figure 8 shows the streamwise extent, i.e., band width, of both TTBs observed in Fig. 7(b) as a function of time. The band width only shows minute variations with time, implying that the statistical equilibrium regime is reached. We note that even at equilibrium one of the TTBs is shorter than the other, a fact corroborated also for $\mathrm{Re_w}$ =950 and 850. On the other hand, the size of both TTBs decreases monotonically with $\mathrm{Re_w}$, as shown in Fig. 9(a). Figure 9(b) shows the equilibrium turbulent fraction vs. $\mathrm{Re_w}$, with fixed $h/d = 0.2$, for the DNSs with the long domain and the reference domain. A decrease in the width of TTB is also observed for DNSs in shorter domains, where only one TTB is present. In the reference domain, the band width is about half of that in the long domain.

The band width determined for the long domain DNS can be as large as $180d$, which is much larger than the original reference domain. From Fig. 9(a) we can infer that the dependence of the mean band width on $\mathrm{Re_w}$ still depends on the length of the computation domain. However, Fig. 9(b) demonstrates that the turbulent fraction does *not*, in turn, depend on the dimensions of the computational domains once they are long enough. This is also true, to some extent, for the determination of the critical Reynolds number. When $\mathrm{Re_w}$ is further decreased from 850 to 800 only one TTB survives in the long domain DNS, whereas for $\mathrm{Re_w} = 750$ the flow is fully laminar. For comparison, in the shorter domain no turbulence is left for $\mathrm{Re_w} = 800$. In both domains, the decrease of F_t with $\mathrm{Re_w}$ follows the same curve, yet longer domains allow for lower equilibrium values of F_t to be reached at lower Reynolds numbers. For instance, F_t can get as low as ≈ 0.1 for $\mathrm{Re_w} = 800$. The figure also suggests that the turbulent fraction can be made arbitrary small by extending the computational domain, until about $\mathrm{Re_w} = 750$ when the flow completely relaminarizes. Hence, longer domains are in principle required for the correct quantitative estimation of the onset Reynolds number, below which no TTB is found. In practice, however, a clear linear scaling of F_t vs. $\mathrm{Re_w}$ emerges from Fig. 9(b), that is apparently independent on the length

[DOI: 10.1299/jfst.2018jfst0019]

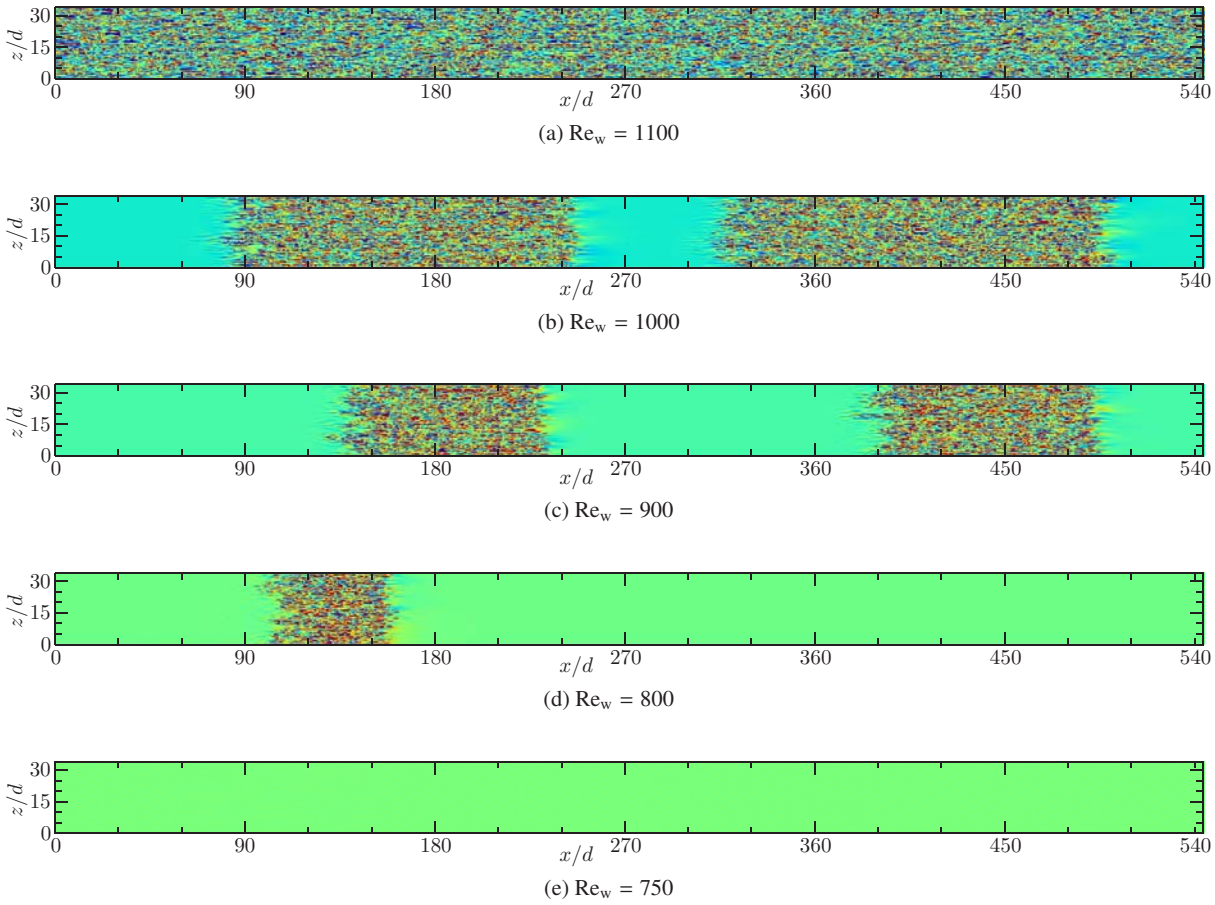

(a) $\mathrm{Re_w}$ = 1100

(b) $\mathrm{Re_w}$ = 1000

(c) $\mathrm{Re_w}$ = 900

(d) $\mathrm{Re_w}$ = 800

(e) $\mathrm{Re_w}$ = 750

Fig. 7 Same as Fig. 6, inside a longer domain. Contours range from $-0.15U_\mathrm{w}$ (blue) to $0.15U_\mathrm{w}$ (red).

of the domain. Extrapolation of F_t towards zero indicates in both cases a critical value of $\mathrm{Re_w}$ around 750. It thus appears that a similar master curve for $F_\mathrm{t}(\mathrm{Re_w})$, linear at its origin, underlies all the simulations of the TTB independently of the domain size. A similar conclusion holds for the (approximate) value of the onset Reynolds number below which no TTB is found.

4. Conclusions

We performed DNS of plane Couette flows using the Busse–Sandham model with one rough wall, with an emphasis on the laminar-turbulent coexistence observed in most subcritical planar shear flows. As in Ishida et al. (2017), the transitional regime features TTBs (transverse turbulent bands) when the roughness height h is sufficiently high, whereas OTBs (oblique turbulent bands) are found in cases with lower h. We have demonstrated that TTBs persist if the computational domain is further enlarged, proving that the non-obliqueness is a robust feature of sufficiently rough walls. The TTBs in the present conditions have a streamwise extent as large as 50–180 gap widths, which shrinks as the Reynolds number decreases. The role of the three-dimensional large-scale flows for their sustenance process and for the explanation of the upstream-downstream asymmetry remains to be investigated. Furthermore, the asymmetry of the mean velocity profile suggests that similar localized turbulent structures could potentially be found in other asymmetric systems, such as wall-bounded flows with differential heating or density stratification. In DNSs with narrow but very long computational domains carried out in the regime of TTBs, the converged turbulent fraction decreases linearly with $\mathrm{Re_w}$. A TTB can even be sustained when the mean turbulent fraction gets as low as 10%. Such a linear dependence of the turbulent fraction with $\mathrm{Re_w}$ was never reported in any other shear flow investigation. We further observe that the mean large-scale spanwise flows typical of OTBs are not found for TTBs, emphasizing how the topology of large-scale flows is closely coupled to the shape of the turbulent patches. The present flow chart determined using a simple roughness model calls for further validation from either new experiments, or full model-free DNS with resolved roughness elements.

[DOI: 10.1299/jfst.2018jfst0019]

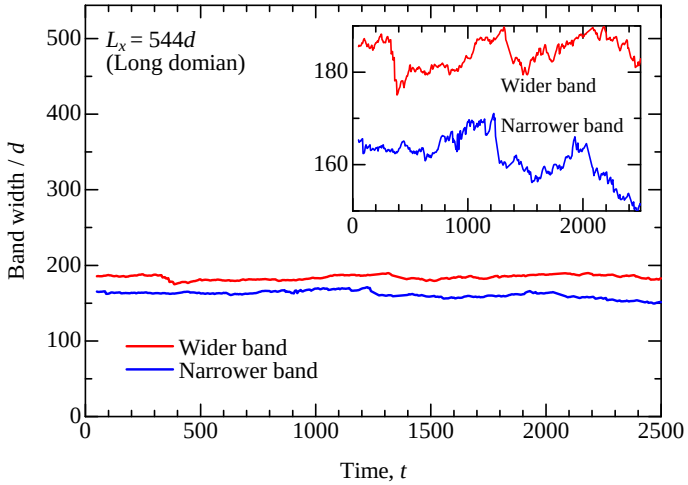

Fig. 8 Time series of the band width of the two TTBs observed at $\mathrm{Re_w} = 1000$ in the long domain, cf. Fig. 7(b). The band width and the time t are normalized by d and d/U_w, respectively. Here, time $t = 0$ is an arbitrary instant after reaching an equilibrium state.

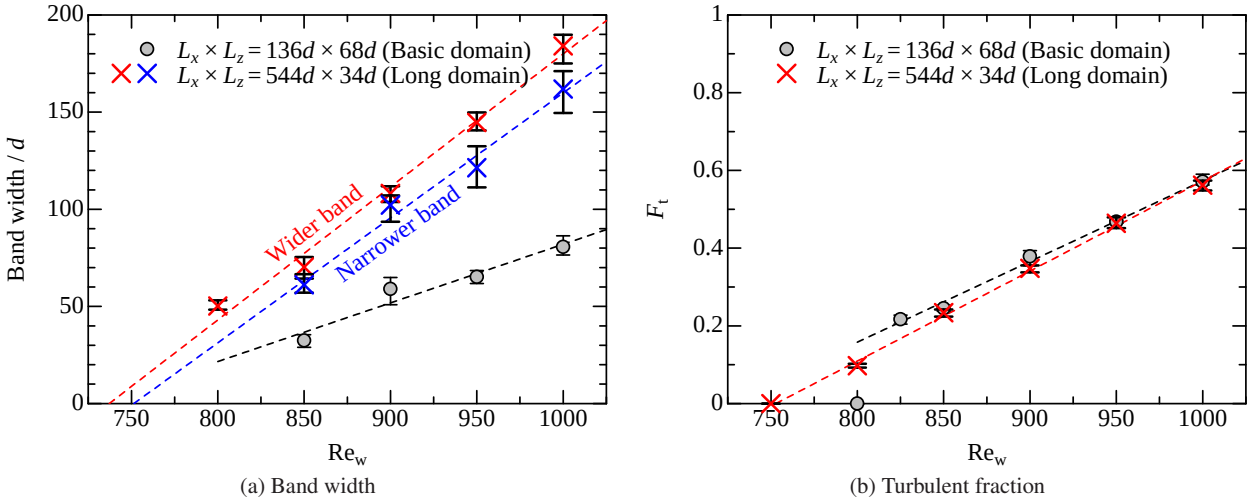

(a) Band width (b) Turbulent fraction

Fig. 9 Reynolds number dependence of the band width of the TTB and mean turbulent fraction for $h/d = 0.2$. Error bars indicate the maximum and minimum values over the computational observation time ($= 2500d/U_\mathrm{w}$). Dotted straight lines are obtained by least-square fitting.

Acknowledgments

This work was partially supported by Grant-in-Aid for Young Scientists (A) #16H06066 from JSPS (Japan Society for the Promotion of Science). G.B. received support from the Swedish Research Council (grant number 621-2016-03533). The present simulations were performed using SX-ACE at the Cyberscience Centre of Tohoku University and at the Cybermedia Centre of Osaka University. We thank JSPS and CNRS (Centre National de la Recherche Scientifique) for additional financial support.

References

Barkley, D., and Tuckerman, L.S. Computational study of turbulent laminar patterns in Couette flow, Physical Review Letters, Vol. 94 (2005), 014502.

Brethouwer, G., Duguet, Y., and Schlatter, P., Turbulent-laminar coexistence in wall flows with Coriolis, buoyancy or Lorentz forces, Journal of Fluid Mechanics, Vol. 704 (2012), pp. 137–172.

Busse, A. and Sandham, N.D., Parametric forcing approach to rough-wall turbulent channel flow, Journal of Fluid Mechanics, Vol. 712 (2012), pp. 169–202.

[DOI: 10.1299/jfst.2018jfst0019]

Chantry, M., Tuckerman, L.S., and Barkley, D. Universal continuous transition to turbulence in a planar shear flow, Journal of Fluid Mechanics, 824 (2017), R1.

Couliou, M. and Monchaux, R., Growth dynamics of turbulent spots in plane Couette flow, Journal of Fluid Mechanics, Vol. 819 (2017), pp. 1–20.

Duguet, Y. and Schlatter, P., Oblique laminar-turbulent interfaces in plane shear flows, Physical Review Letter, Vol. 110 (2013), 034502.

Duguet, Y., Schlatter, P., and Henningson, D.S., Formation of turbulent patterns near the onset of transition in plane Couette flow, Journal of Fluid Mechanics, Vol. 650 (2010), pp. 119–129.

Finnigan, J.J., Shaw, R.H., and Patton, E.G., Turbulence structure above a vegetation canopy, Journal of Fluid Mechanics, Vol. 637 (2009), pp. 387–424.

Ishida, T., Brethouwer, G., Duguet, Y., and Tsukahara, T., Laminar-turbulent patterns with rough walls, Physical Review Fluids, Vol. 2 (2017), 073901.

Lemoult, G., Shi, L., Avila, K., Jalikop, S.V., Avila, M., and Hof, B., Directed percolation phase transition to sustained turbulence in Couette flow, Nature Physics, Vol. 12 (2016), pp. 254–258.

Manneville, P., Transition to turbulence in wall-bounded flows: Where do we stand?, Mechanical Engineering Reviews, Vol. 3 (2016), 15-00684, DOI:10.1299/mer.15-00684.

Manneville, P. and Rolland, J., On modelling transitional turbulent flows using under-resolved direct numerical simulations: the case of plane Couette flow, Theoretical and Computational Fluid Dynamics, Vol. 25 (2011), pp. 407–420.

Mukund, V. and Hof, B., The critical point of the transition to turbulence in pipe flow. Journal of Fluid Mechanics, Vol. 839 (2018), pp. 76–94.

Prigent, A., Grégoire, G., Chaté, H., Dauchot, O., and van Saarlos, W., Large-scale finite-wavelength modulation within turbulent shear flows, Physical Review Letter, Vol. 89 (2002), 014501.

Sano, M. and Tamai, K., A universal transition to turbulence in channel flow, Nature Physics, Vol. 12 (2016), pp. 249–253.

Shi, L., Avila, M., and Hof, B. Scale invariance at the onset of turbulence in Couette flow. Physical Review Letters, Vol. 110 (2013), 204502.

Su, H.-B., Shaw, R.H., Paw K.T., Moeng, C.-H., and Sullivan, P.P., Turbulent statistics of neutrally stratified flow within and above a sparse forest from large-eddy simulation and field observations, Boundary-Layer Meteorology, Vol. 88 (1998), pp. 363–397.

Tsukahara, T., Structures and turbulent statistics in a rotating plane Couette flow, Journal of Physics: Conference Series, Vol. 318 (2011), 022024.

Tsukahara, T., Kawamura, H., and Shingai, K., DNS of turbulent Couette flow with emphasis on the large-scale structure in the core region, Journal of Turbulence 7 (2006), N19.

Tsukahara, T., Kawaguchi, Y., and Kawamura, H., DNS of turbulent plane Couette flow with emphasis on turbulent stripe, Advances in Turbulence XII (2009), Springer Berlin, pp. 71–73, DOI:10.1007/978-3-642-03085-7_16.

Tsukahara, T., Tillmark, N., and Alfredsson, P.H., Flow regimes in a plane Couette flow with system rotation, Journal of Fluid Mechanics, Vol. 648 (2010), pp. 5–33.

Tuckerman, L.S. and Barkley, D., Patterns and dynamics in transitional plane Couette flow, Physics of Fluids, Vol. 23 (2011), 041301.

[DOI: 10.1299/jfst.2018jfst0019]